A Theoretical Investigation on the Kinetics and Mechanism of the Reaction of Amidogen with Hydroxyl Radical

S. Hosein Mousavipour,* Fatemeh Pirhadi, and Arezoo HabibAgahi

Department of Chemistry, College of Sciences, Shiraz University, Shiraz, 71454, Iran

Received: June 3, 2009; Revised Manuscript Received: September 7, 2009

The kinetics and mechanism of the reaction between amidogen radical and hydroxyl radical have been theoretically investigated on the lowest singlet and triplet surfaces. The singlet surface consists of two long-lived chemically activated NH_2OH^* and NH_3O^* intermediates with 10 different channels. A hydrogen abstraction channel on the triplet surface proceeds through van der Waals complex in both reactant side and product side to produce $NH_3 + O(^3P)$. The effect of multiple reflections of the van der Waals complexes on the rate constant is investigated. Multichannel RRKM-TST calculations have been carried out to calculate the individual rate constants for the formation of those products that proceed through activated adducts on the singlet surface. The rate constants for direct hydrogen abstraction reactions were calculated by using direct-dynamics canonical variational transition-state theory with small curvature approximation for tunneling.

Introduction

Amidogen and hydroxyl radicals are two important reactive radicals in the atmospheric processes and combustion chemistry. Hydroxyl radical and amidogen play an important role in the NO_x process and in the gas-phase oxidation of ammonia.[1−3] The reactions of NH_x species with H_yO species have been investigated by several experimental and theoretical studies, and have been reviewed to some extent, yet more accurate studies are still needed to clarify the mechanism and to find more accurate rate constants for the individual reactions involved in these systems.[2]

The kinetics of reaction of $NH_2 + OH$ has been studied by different groups.[4−24] On the basis of the results from the previous studies that have been reported in the literatures and our theoretical results, a possible mechanism for the title system on both singlet and triplet surfaces is shown in Scheme 1.

Reactions R1−R10 occur on the singlet surface and reactions R11 and R12 occur on the triplet surface. The proposed mechanism (based on the nature of the reactions) might be classified into two kinds of reactions. Direct hydrogen abstraction channels that occur on both singlet and triplet surfaces, reactions R9−R12, and those channels that proceed through the formation of energized adducts NH_2OH^* and NH_3O^* that are followed by bond cleavage or rearrangement reactions on the singlet surface, reactions R1−R8.

Fagerstrom et al.[4] have studied the kinetics of the title reaction in a pulse radiolysis experiment. They have only monitored the consumption of the reactants in their study with no analysis of the products. They did not observe any pressure dependency for the reaction between 375−750 Torr and over the temperature range of 200−400 K. They reported a high pressure limiting rate constant expression for consumption of the reactants as $k_{obs} = (1.8 \pm 0.3) \times 10^{10}\ T^{0.2}$ L mol^{-1} s^{-1}. Gericke et al.[5] in a photodissociation dynamics study of NH_2OH suggested that the main dissociation channels would lead to $2H + HNO$ and $NH_2 + OH$ production. Kimball-Linne and Hanson[6] in a flow reactor study suggested a value of 6×10^9 L mol^{-1} s^{-1} for k_{12} in a temperature range of 1050−1400 K. Cohen and Westberg[7] in a literature review have suggested rate constant expressions for reaction R11 as $k_{11} = 1.1\ T^{2.6}$ exp(7.2 kJ/RT) L mol^{-1} s^{-1} at 298−2000 K and for reaction R12 as $k_{12} = 9.0 \times 10^4\ T^{1.5}$ exp(1.9 kJ/RT) L mol^{-1} s^{-1} over the temperature range of 250−3000 K. On the basis of a literature review, Baulch et al.[8] have reported the rate constant expression $k_{11} = 1.99 \times 10^7\ T^{0.41}$ exp(−2.08 kJ/RT) L mol^{-1} s^{-1} for reaction R11 over the temperature range of 500−2500 K. Dean and Bozzelli have made an extensive review of theoretical and experimental data on reaction R12.[9]

SCHEME 1

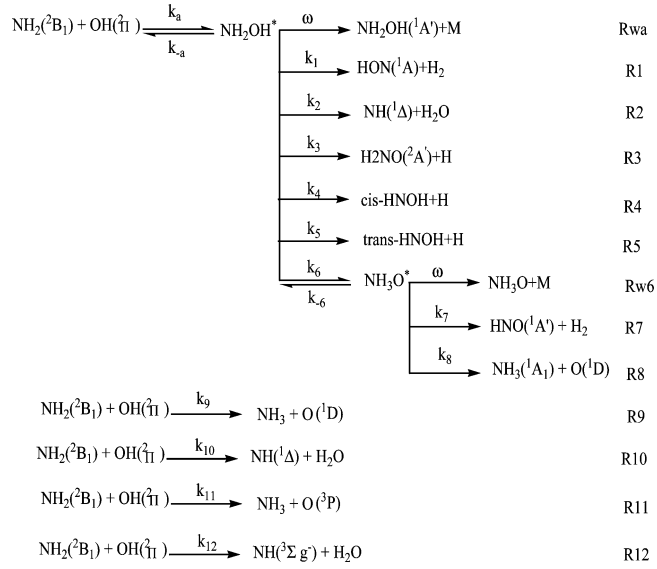

Four short-lived van der Waals complexes $H_2N\cdots HO$ and $H_2NH\cdots O$ on the triplet surface and $HN\cdots OH_2$ and $H_2NH\cdots O$ on the singlet surface are involved in this system. Mackie et al.[10] have studied the mechanism of the reaction between NH and H_2, H_2O, and CO_2 on both singlet and triplet surfaces. In their suggested mechanism for the reaction of $NH + H_2O$, only the formation of van der Waals complex $HN\cdots OH_2$ on the singlet surface is predicted and reaction R11 on the triplet

* E-mail: mousavi@susc.ac.ir.

10.1021/jp905197h CCC: $40.75
Published on Web 10/09/2009

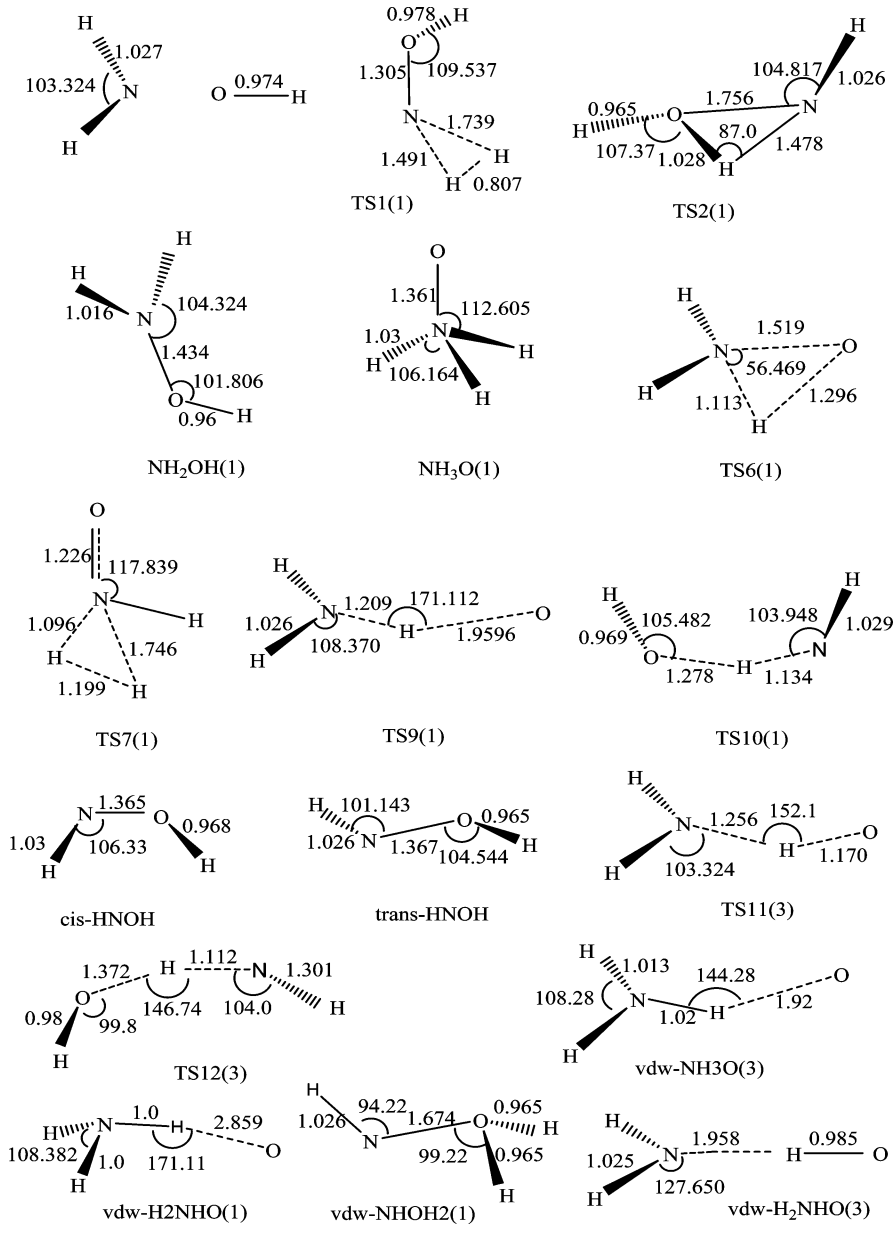

Figure 1. Optimized geometries of the stationary points at the B3LYP/6-311++G(3df,3p) level.

surface to produce $NH_3 + O(^3P)$ is ignored in their proposed mechanism, although reaction R8 to produce $NH_3 + O(^1D)$ with much higher potential barrier on the singlet surface is reported. They did not include reactions R9 and R10 in their suggested mechanism. Xu et al.[11] have used variational transition state theory to study the dynamical properties of the hydrogen abstraction reaction R12 at three different levels of theory. Shu et al.[12] in a crossed molecular beam studies of the $O(^1D) + NH_3$ reaction reported $NH_2 + OH$, $NH_2O + H$, and cis and trans of HNOH + H as the products, where OH formation (the reverse of reaction R9) was the dominant channel. They used time-of-flight spectroscopy to detect the products. They have reported formation of NH_2OH is the first step in the reaction of NH_3 with atomic oxygen. They did not report detection of amine oxide NH_3O. The reason that NH_3O was not being detected by these authors might have been due to the identical mass of NH_3O and NH_2OH. Wang et al.[13] in a theoretical study on the kinetics of the $O(^1D) + NH_3$ reported the formation of the two van der Waals complexes $H_2NH\cdots O$ and $HN\cdots OH_2$ on the singlet surface. Their calculations at the MRCI/6-311+G(3df,2p)//CASSCF/6-311G(d,p) level show a slightly negative relative energy -1.7 kJ mol^{-1} of $H_2NH\cdots O$ complex with respect to the $NH_3 + O(^1D)$. They concluded that the existence of this complex as a local minimum on the first excited PES could be an artifact of the theoretical method they used. Although, they reported the formation of chemically activated intermediate NH_2OH^*, the formation of another intermediate amine oxide NH_3O^*[14] was ignored in their suggested mechanism. They suggested formation of NOH + H_2 and NH + H_2O (the products of channels R1 and R2 or R10) are the minor path and suggested the reason that H_2O and H_2 were not being detected by Shu et al.[12] was due to the identical mass of H_2O and NH_3 and negligible amount of H_2 produced in their experiment. They have reported the branching ratio for the dissociation of NH_2OH into the possible channels on the singlet surface without including the rearrangement reaction for the formation of energized intermediate NH_3O with a lower potential barrier than the other reported channels. Obviously, neglecting the role of NH_3O formation in this system would lead to inaccurate branching ratios.

This multichannel system consists of two deep potential energy wells on the singlet surface. Understanding the dynamics

TABLE 1: Relative Energies Corrected for Zero-Point Energies of Various Species at Different Levels of Theory in kJ mol^{-1} [a]

species	B3LYP[b]	B3LYP	CCSD(T)	CCSD(full)	MPWB1K	ZPE[c]
$NH_2(^2B_1)$ + OH ($^2\Pi$)*	0.0	0.0	0.0	0.0	0.0	72.0
vdw-$HNOH_2$(S)	11.1	12.3	3.3	19.7		97.2
TS1(S)	109.6	111.9	118.6	144.3		74.3
TS2(S)	20.9	21.5	10.2	32.3		88.1
TS6(S)	−40.2	−40.9	−46.0	−26.4		92.4
TS7(S)	64.3	66.2	65.8	106.1		77.7
TS9(S)	261.6	261.0	246.6	269.1		84.7
vdw-H2NHO(S)	256.8	256.3	199.8	218.1		97.5
TS11(T)	0.3	0.4	22.8	32.0	9.4	75.0
TS12(T)	−17.3	−15.6	0.7	13.9		74.5
TS10(S)	150.0	152.5	31.1	191.4		71.3
NH_2OH	−241.2	−238.5	−247.3	−238.2		105.9
$NH(^3\Sigma_g^-)$ + H_2O	−87.7	−80.5	−95.6	−92.5		86.7
$NH(^1\Delta)$ + H_2O	122.0	129.1	87.4	104.4		86.9
NH_3 + $O(^3p)$*	1.7	0.2	−16.0	−15.7	−29.9	89.7
NH_3 + $O(^1D)$	264.1	265.6	196.7	217.0		89.7
$HNO(^1A')$ + H_2	−91.6	−89.0	−102.7	−81.3		66.4
$HON(^1A)$ + H_2	74.5	77.5	70.3	93.0		65.0
$H_2NO(^2A')$ + H	60.2	62.4	69.1	75.6		69.1
cis-$HNOH(^2A'')$ + H	121.8	124.1	118.6	130.2		68.9
trans-$HNOH(^2A'')$ + H	100.8	103.0	97.3	108.4		70.8
vdw-H_2NHO(T)	−16.1	−15.6	−16.4	−17.6	−19.3	81.2
NH_3O(S)	−143.3	−142.4	−143.6	−133.1		106.4
vdw-NH_3O(T)	−8.7	−9.3	−19.6	−18.4		90.8

[a] Along with Aug-cc-pVTZ basis set. [b] Calculated at the 6-311++G(3df,3p) basis set. [c] Calculated at the B3LYP/6-311++G(3df,3p) level.

of chemical reactions consisting of multichannels with deep potential energy wells is of great importance. In contrast to the previous studies on this system, the individual rate constants for different paths on the singlet surface are calculated independently, we believe that the rate of each path should be calculated in the presence of the other paths to include the effect of each path on the rate of the other paths.

In the present study, a detailed reaction mechanism for both lowest singlet and triplet surfaces is investigated by including more possible channels than what is reported in literature to date. The calculations show that the reaction mechanism for this system is much more complicated than what was expected previously. We were also interested to investigate the effect of short-lived van der Waals complexes on the kinetics of this system.

We have used a method based on RRKM method and transition state theory (TST) to calculate the rate constants for reactions R1 to R8 that proceed through two vibrationally energized adducts.[25,26] The rate constants for reactions R9 to R12 that possess a potential barrier were calculated by means of canonical variational transition state theory (CVT).

Discussion and Results

Ab Initio Calculations. Ab initio calculations were performed using the Gaussian 03 program.[27] The geometries of the reactants, transition states, intermediates, and products were optimized by the hybrid density functional B3LYP method (Becke's three parameter nonlocal exchange functional[28] with the nonlocal correlation functional of Lee, Yang, and Parr[29]) along with the 6-311++G(3df,3p) basis set. The single point CCSD/Aug-cc-pVTZ//mp2/Aug-cc-pVTZ calculations were carried out to obtain more accurate energies of the stationary points along the PES. The CCSD calculations were performed full (specifies the inclusion of all electrons in correlation calculations) and also as triple excitation. To annihilate the spin contamination, calculations along some reaction coordinates have repeated by using multiconfiguration self-consistent field (MCSCF) method.[30] Harmonic vibrational frequencies were obtained at the B3LYP/6-311++G(3df,3p) level of theory in order to characterize the stationary points as local minima or first-order saddle points and to obtain zero-point vibration energy (ZPE). Harmonic vibrational term values were scaled by a factor of 0.96. The intrinsic reaction coordinate (IRC) method[31] has been utilized to validate the connection of each transition state to the corresponding minima along the reaction paths.

Geometries and Potential Energy Surfaces. The optimized geometries of the stationary points at the B3LYP/6-311++G(3df,3p) level are shown in Figure 1. The multiplicity of each species is shown in the parentheses. The calculated relative energies at different levels of theory and zero-point energies (ZPEs) are listed in Table 1, where the relative energies are corrected for ZPEs. A schematic potential energy diagram on both singlet and triplet surfaces at the CCSD(full)/Aug-cc-pVTZ level is presented in Figure 2. Vibrational term values and moments of inertia for all species are listed in Table 2.

The association reaction of NH_2 with OH by a barrierless process forms vibrationally excited NH_2OH* intermediate, which is 238.2 kJ mol^{-1} more stable than the reactants at the CCSD(full) level. As shown in Figure 2, energized intermediate NH_2OH* passes over saddle point TS6 with 211.8 kJ mol^{-1} barrier height at the CCSD(full) level via a [1,2] hydrogen shift to form another energized intermediate NH_3O* that is 133.1 kJ mol^{-1} more stable than the reactants on the singlet surface or dissociates to the corresponding products of reactions R1 to R5. Each of the two energized intermediates NH_2OH* and NH_3O* dissociate according to different channels as shown in Figure 2 or stabilize under collision via channels Rwa and Rw6 in our suggested mechanism, respectively. Baulch et al.[32] in an experimental study on the kinetics of reaction between NH_3 and O suggested formation of NH_3O as an intermediate species that rearranges to hydroxylamine. Kirby et al.[33] reported the existence of NH_3O as a stable molecule in a crystal structure and as a likely reactive species in many reactions of hydroxylamine. To the best of our knowledge, no direct observation of gas phase NH_3O has been reported to date.

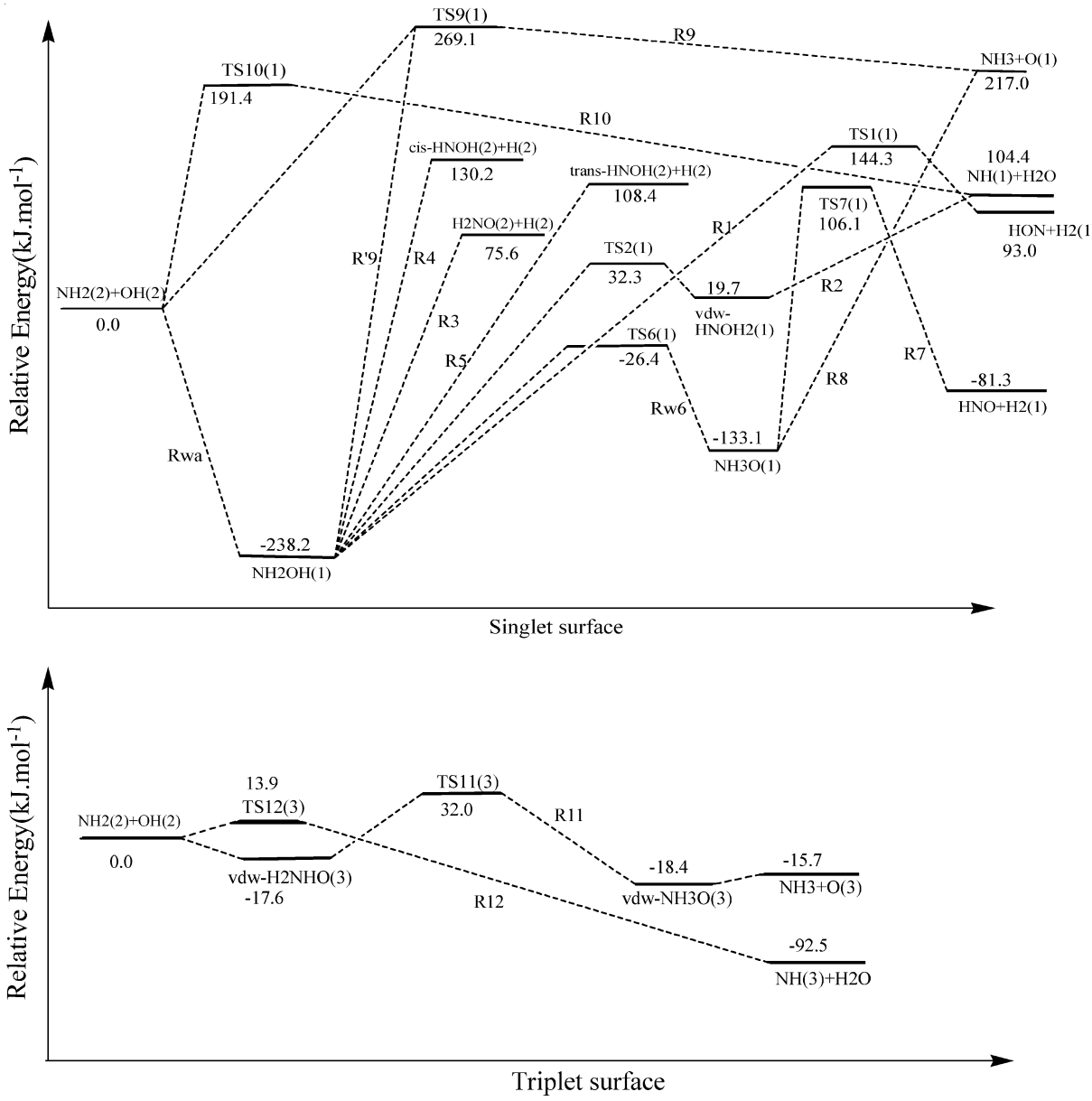

Figure 2. Relative energies of the stationary points in kJ mol^{-1} on both singlet and triplet surfaces at the CCSD(full)/Aug-cc-pVTZ level. All values are corrected for the zero-point energies.

The internally excited NH_2OH^* can dissociate via TS1 producing $HON(^1A) + H_2$ in a concerted hydrogen molecule elimination mechanism. Reaction R2 occurs via a concerted mechanism that one of the hydrogen atoms in NH_2OH^* migrates from nitrogen to oxygen while N−O bond lengthening to produce $HN{\cdot}OH_2$ van der Waals complex to en route $NH(^1\Delta) + H_2O$. The van der Waals complex $HN{\cdot}OH_2$ is 12.6 kJ mol^{-1} more stable than TS2 and 84.7 kJ mol^{-1} more stable than $NH(^1\Delta) + H_2O$ products. The effect of the presence of this complex on the rate of formation of $NH(^1\Delta) + H_2O$ products will be discussed later.

Two channels R7 and R8 take place by decomposition of energized intermediate amine oxide NH_3O^*, H_2-elimination to form $HNO(^1A') + H_2$ or N−O bond cleavage to produce $NH_3 + O(^1D)$.

Two possible channels exist for the formation of $NH_3 + O(^1D)$ on the singlet surface, reactions R8 and R9. Reaction R9 proceeds by passing over high potential energy TS9 with 269.1 kJ mol^{-1} barrier height. Two pathways were predicted for the formation of TS9. The first path is direct association of the reactants, and the second path is the NH_2OH^* rearrangement channel, as shown by R′9 in Figure 2. We ignored the contribution of channel R′9 in calculating the total rate constant of disappearance of NH_2OH^* because of its higher barrier height relative to the other channels. In agreement with Wang et al.,[13] we found van der Waals complex $H_2NH\cdots O$ along the reaction coordinate from TS9 toward the formation of $NH_3 + O(^1D)$ only at the CASSCF level. We were not able to detect any local minima along this channel at the other levels of theory. The contribution of both channels R8 and R9 should be negligible in this system. Two possible channels exist for the formation of $NH + H_2O$ on the singlet surface, reactions R2 and R10. Reaction R10 passes over TS10 with 191.4 kJ mol^{-1} barrier height that should be a minor path in comparison with reaction R2.

In this system, atomic oxygen and NH radicals are produced on both singlet and triplet surfaces in this system. Although $O(^3P)$ and $NH(^3\Sigma_g^-)$ radical are 196.9 and 232.7 kJ mol^{-1} more stable than $O(^1D)$ and $NH(^1\Delta)$ at the CCSD(full) level, respectively, the formation of triplet species on the singlet

TABLE 2: Vibrational Frequencies and Moments of Inertia of Different Species Calculated at the at the B3LYP/6-311++G(3df,3p) Level and Scaled by 0.96

species	frequencies (cm^{-1})	I_i (a.u.)		
NH_2	1468.4, 3221.4, 3307.3	0.72	1.31	2.02
OH	3563.8	0.90	0.90	0.00
vdw-H_2NHO(T)	155.5, 177.1, 180.6,499.9, 615.0, 1466.9, 3247.6, 3336.5, 3345.8	1.33	74.04	75.37
TS1(S)	392.7, 634.8, 829.5, 947.4, 1125.6, 1366.0, 3269.0, 3361.0, −810.1	4.41	18.37	20.66
TS2(S)	484.8, 544.4, 794.2, 1167.1, 1441.0, 2794.4, 3266.0, 3653.5, −890.0	2.57	26.11	26.83
TS7(S)	707.3, 841.8, 1142.4, 1257.0, 1412.3, 1552.6, 2527.2, 3035.8, −1190.4	3.41	17.51	18.69
TS9(S)	343.3, 513.8, 1212.0, 1315.7, 1495.5, 1688.4, 3733.4, 3852.5, −1197.5	1.81	82.42	83.26
vdw-H_2NHO(S)	48.7, 101.7, 122.4, 1099.0, 1799.3, 1800.8, 3690.2, 3818.1, 3820.4	1.82	122.2	123.1
TS11(T)	411.3, 448.2, 725.5, 1026.5, 1253.2, 1516.7, 3289.3, 3371.7, −1385.0	2.03	46.09	46.72
TS12(T)	385.8, 414.5, 678.4, 1042.2, 1191.8, 1679.3, 3414.9, 3653.2, −2234.4	2.05	46.12	46.58
TS10(S)	78.4, 411.3, 772.6, 806.3, 881.0, 1650.7, 3471.5, 3847.3, −1253.8	1.53	50.65	51.46
TS6(S)	756.2, 970.2, 1022.7, 1151.1, 1508.9, 2647.6, 3335.2, 3443.2, −1588.6	2.65	21.02	21.27
NH_2OH(S)	397.8, 912.3, 1101.7, 1282.2, 1348.9, 1601.6, 3301.5, 3374.0, 3685.0	2.62	19.68	19.72
NH_3O(S)	923.5, 1111.7, 1111.9, 1469.7, 1585.4, 1585.8, 3086.6, 3101.0, 3102.0	2.74	18.65	18.65
vdw-$HNOH_2$(S)	321.4, 480.5, 702.4, 723.3, 1258.6, 1553.0, 3252.7, 3614.1, 3697.0	2.69	25.03	25.29
vdw-NH_3O(T)	150.3, 241.3, 249.5, 876.0,1200.3, 1665.9, 3486.6, 3652.6, 3662.8	2.79	47.93	47.94
H_2NO	283.4, 1219.6, 1328.2, 1593.7, 3272.2, 3396.0	1.57	14.74	16.26
trans-HONH	710.3, 1067.8, 1220.2, 1511.3, 3234.0, 3619.3	1.68	15.82	17.50
cis-HONH	546.5, 1053.2, 1271.6, 1449.6, 3178.2, 3566.1	1.69	15.94	17.63

TABLE 3: Microcanonical Variational RRKM Results for Unimolecular Dissociation Reaction k_{-a}

E $(v,j)^a$	$E^{\#}$ $(v,j)^b$	$R^{\#}$ (Å)^c	$E_0{}^d$	N $(v,j)^e \times 10^4$	G $(E^{\#})^f \times 10^4$	k $(E) \times 10^{11}$ (1/s)
247	34	3.42	213	0.07754	0.09419	0.3642
250	38	3.41	212	0.08387	0.1302	0.4654
252	40	3.39	212	0.08728	0.1512	0.5195
254	42	3.39	212	0.09071	0.1757	0.5807
255	43	3.39	212	0.09430	0.2023	0.6430
257	45	3.38	212	0.09801	0.2343	0.7167
259	47	3.37	212	0.1018	0.2679	0.7888
260	50	3.10	210	0.1059	0.3051	0.8642
269	59	3.07	210	0.1277	0.5649	1.326
279	70	3.04	209	0.1591	1.100	2.071
287	78	3.01	209	0.1903	1.823	2.872
290	81	3.00	209	0.2042	2.210	3.244
299	91	2.97	208	0.2428	3.488	4.308
305	97	2.95	208	0.2782	4.924	5.306
312	104	2.93	208	0.3179	6.835	6.446
320	113	2.91	207	0.3744	10.09	8.081
327	120	2.89	207	0.4259	13.57	9.553

[a] Total energy available to the system in kJ mol^{-1}. [b] Transition state energy in kJ mol^{-1}. [c] Position of the bottleneck in angstrom. [d] Classical energy difference between the reactant and the transition state. [e] Density of states in $1/cm^{-1}$. [f] Sum of states.

TABLE 4: Microcanonical Variational RRKM Results for Unimolecular Dissociation Reaction k_3

E $(v,j)^a$	$E^{\#}$ $(v,j)^b$	$R^{\#}$ (Å)^c	$E_0{}^d$	N $(v,j)^e \times 10^4$	G $(E^{\#})^f \times 10^4$	k $(E) \times 10^{11}$ (1/s)
342	14	2.51	328	0.2306	0.02281	0.002965
346	19	2.49	327	0.2452	0.03815	0.004665
351	25	2.43	326	0.2686	0.07870	0.008784
359	34	2.35	325	0.3120	0.2008	0.01929
366	43	2.29	323	0.3510	0.3713	0.03171
371	49	2.25	322	0.3830	0.5667	0.04436
405	83	2.15	322	0.6873	1.539	0.06714
412.	90	2.14	322.	0.7646	2.940	0.1153

[a] Total energy available to the system in kJ mol^{-1}. [b] Transition state energy in kJ mol^{-1}. [c] Position of the bottleneck in angstrom. [d] Classical energy difference between the reactant and the transition state. [e] Density of states in $1/cm^{-1}$. [f] Sum of states.

surface is spin forbidden and can take place only through singlet−triplet intersystem crossing. We were not able to detect such intersystem crossing points in this system.

Calculation Methods of the Rate Constants. As shown in Figure 2, on the singlet potential energy surface, channels R1−R8 proceed through the formation of energized intermediates of NH_2OH* and NH_3O*. For the formation of energized intermediate NH_2OH* no saddle point was observed. Also, no saddle points were found for reactions R3−R5 and R8. Microcanonical variational RRKM method was used to locate

TABLE 5: Microcanonical Variational RRKM Results for Unimolecular Dissociation Reaction k_4

$E\ (v,j)^a$	$E^{\#}\ (v,j)^b$	$R^{\#}$ (Å)^c	$E_0{}^d$	$N\ (v,j)^e \times 10^4$	$G\ (E^{\#})^f \times 10^4$	$k\ (E) \times 10^{11}$ (1/s)
406	46	2.53	360	0.6919	0.7109	0.03080
411	52.	2.50	359	0.7496	1.058	0.04230
415	57	2.48	358	0.7903	1.348	0.05115
423	66	2.45	358	0.9007	2.370	0.07888
440	82	2.41	358	1.163	4.353	0.1123
461	104	2.38	357	1.601	17.72	0.3319
471	115	2.36	356	1.848	29.93	0.4857
478	123	2.35	355	2.030	41.29	0.6098
487	133	2.33	354	2.280	60.11	0.7903

[a] Total energy available to the system in kJ mol^{-1}. [b] Transition state energy in kJ mol^{-1}. [c] Position of the bottleneck in angstrom. [d] Classical energy difference between the reactant and the transition state. [e] Density of states in 1/cm^{-1}. [f] Sum of states.

TABLE 6: Microcanonical Variational RRKM Results for Unimolecular Dissociation Reaction k_5

$E\ (v,j)^a$	$E^{\#}\ (v,j)^b$	$R^{\#}$ (Å)^c	$E_0{}^d$	$N\ (v,j)^e \times 10^4$	$G\ (E^{\#})^f \times 10^4$	$k\ (E) \times 10^{11}$ (1/s)
377	10	2.80	367	3.080	0.01827	0.001779
378	12	2.79	366	3.168	0.02856	0.002702
382	17	2.75	365	3.352	0.05227	0.004675
383	19	2.73	364	3.447	0.07099	0.00617
387	23	2.69	364	3.644	0.1142	0.0094
390	27	2.66	363	3.851	0.1770	0.01378
392	30	2.64	362	3.959	0.2159	0.01635
393	31	2.63	362	4.069	0.2613	0.01925
395	34	2.61	361	4.181	0.3127	0.02242
400	40	2.57	360	4.536	0.5092	0.03366
402	43	2.56	359	4.660	0.5924	0.03812
412	55	2.50	357	5.466	0.1339	0.07343
418	62	2.47	356	6.069	0.2158	0.1066
425	70	2.44	355	6.730	0.3351	0.1493
432	74	2.42	358	7.452	0.3041	0.1223
447	90	2.41	357	9.330	0.9219	0.2962
450	94	2.40	356	9.799	0.1138	0.3482

[a] Total energy available to the system in kJ mol^{-1}. [b] Transition state energy in kJ mol^{-1}. [c] Position of the bottleneck in angstrom. [d] Classical energy difference between the reactant and the transition state. [e] Density of states in 1/cm^{-1}. [f] Sum of states.

TABLE 7: Microcanonical Variational RRKM Results for Unimolecular Dissociation Reaction k_8

$E\ (v,j)^a$	$E^{\#}\ (v,j)^b$	$R^{\#}$ (Å)^c	$E_0{}^d$	$N\ (v,j)^e \times 10^4$	$G\ (E^{\#})^f \times 10^4$	$k\ (E) \times 10^{11}$ (1/s)
419	5	3.54	400	0.1507	0.092	0.0184
430	8	3.46	398	0.1801	0.36	0.059
435	9	3.41	398	0.1942	0.55	0.086
444	11	3.37	397	0.2197	1.1	0.15
447	12	3.36	396	0.2308	1.4	0.18
464	16	3.22	393	0.2934	4.1	0.42
466	18	3.21	392	0.3004	4.5	0.45
499	27	3.00	386	0.4750	24	1.5
508	29	2.99	385	0.5364	36	2
541	38	2.94	383	0.8133	120	4.4
552	41	2.92	382	0.9300	170	5.5
584	50	2.84	377	1.372	450	9.9
598	53	2.81	375	1.616	670	12
626	61	2.76	371	2.201	1300	18
643	65	2.73	369	2.639	1900	22
651	68	2.71	367	2.885	2300	24
663	76	2.50	343	3.26	2900	27

[a] Total energy available to the system in kJ mol^{-1}. [b] Transition state energy in kJ mol^{-1}. [c] Position of the bottleneck in angstrom. [d] Classical energy difference between the reactant and the transition state. [e] Density of states in 1/cm^{-1}. [f] Sum of states.

the positions of the bottlenecks for the entrance channel of the energized intermediate NH_2OH and formation of the products of reactions R3−R5 from hydroxyl amine and reaction R8 from amine oxide.

To estimate the rate constants for individual unimolecular reaction steps the variational RRKM[34] and TST calculations have been carried out. Vibrationally excited intermediate NH_2OH^* can be stabilized under collision, reaction Rwa, or proceed through dissociation channels R1−R5, or formation of energized intermediate NH_3O^*. Energized intermediate NH_3O^* can be stabilizes according to reaction Rw6 or dissociates via reactions R7 and R8.

As shown in Figure 2, channels R9 and R10 on the singlet surface and channels R11 and R12 on the triplet surface pass over the corresponding saddle points TS9, TS10, TS11, and TS12, respectively. Canonical variational transition state theory (CVT) calculations were performed to calculate the rate constants for these channels. GAUSSRATE9.1[35] program, which is an interface between POLYRATE9.3.1[36] and Gaussian 03, was employed in our CVT calculations.

Rate Constant Calculations for Channels R1−R8. The results from the CCSD(full)/Aug-cc-pVTZ calculations were used to calculate the rate constants. The necessary data for RRKM calculations are summarized in Tables 1 and 2.

Microcanonical variational RRKM calculations are carried out to locate the position of the bottlenecks for those channels with no saddle point. Tables 3−7 show the results of microcanonical variational RRKM calculations for the entrance channel of NH_2OH^* formation and reactions R3−R5, and R8, respectively. To locate the position of bottleneck, the RRKM program searches for the minimum in the sum of states versus reaction coordinate as a function of available energy (temperature).[37] A standard RRKM program by Zhu and Hase[38] was used to calculate the sum and density of states.

In RRKM calculations, a step size of $\Delta E^+ = 0.2$ kJ mol^{-1} was used. In these calculations the external rotations were treated as being adiabatic. The ratio of the electronic partition functions was assumed to be equal 1. N_2 was chosen as bath gas and a value of 0.2−0.5 was selected for the collision efficiency β_c from ref 39. Sum of states was calculated according to Tardy et al.[40] method, in which only a fraction of the zero-point energy (aE_z) is included in the classical energy at each point along the reaction coordinate.

The rate constants for channels R1−R8 were calculated according to a method suggested by Dean,[25] which is based on RRKM method. Steady-state assumption for the energized intermediates leads to the following expressions for the second-order rate constants of channels R1−R8.

$$k_{bi}(R1) = \kappa\frac{\sigma B_e Q_a^{\neq}}{hQ_{NH_2}Q_{OH}}\sum_{E0}^{\infty}\frac{k_1(E)\,D'\{G(E^+)\}\exp(-E^+/RT)}{DD' - k_6(E)\,k_{-6}(E)}$$

$$k_{Wa} = \kappa\frac{\sigma B_e Q_a^{\neq}}{hQ_{NH_2}Q_{OH}}\sum_{E0}^{\infty}\frac{wD'\{G(E^+)\}\exp(-E^+/RT)}{DD' - k_6(E)\,k_{-6}(E)}$$

$$k_{bi}(R2) = \kappa\frac{\sigma B_e Q_a^{\neq}}{hQ_{NH_2}Q_{OH}}\sum_{E0}^{\infty}\frac{k_2(E)\,D'\{G(E^+)\}\exp(-E^+/RT)}{DD' - k_6(E)\,k_{-6}(E)}$$

$$k_{bi}(R3) = \kappa\frac{\sigma B_e Q_a^{\neq}}{hQ_{NH_2}Q_{OH}}\sum_{E0}^{\infty}\frac{k_3(E)\,D'\{G(E^+)\}\exp(-E^+/RT)}{DD' - k_6(E)\,k_{-6}(E)}$$

$$k_{bi}(R4) = \kappa\frac{\sigma B_e Q_a^{\neq}}{hQ_{NH_2}Q_{OH}}\sum_{E0}^{\infty}\frac{k_4(E)\,D'\{G(E^+)\}\exp(-E^+/RT)}{DD' - k_6(E)\,k_{-6}(E)}$$

$$k_{bi}(R5) = \kappa\frac{\sigma B_e Q_a^{\neq}}{hQ_{NH_2}Q_{OH}}\sum_{E0}^{\infty}\frac{k_5(E)\,D'\{G(E^+)\}\exp(-E^+/RT)}{DD' - k_6(E)\,k_{-6}(E)}$$

$$k_{6w} = \kappa\frac{\sigma B_e Q_a^{\neq}}{hQ_{NH_2}Q_{OH}}\sum_{E0}^{\infty}\frac{wk_6(E)\{G(E^+)\}\exp(-E^+/RT)}{DD' - k_6(E)\,k_{-6}(E)}$$

$$k_{bi}(R7) = \kappa\frac{\sigma B_e Q_a^{\neq}}{hQ_{NH_2}Q_{OH}}\sum_{E0}^{\infty}\frac{k_6(E)\,k_7(E)\{G(E^+)\}\exp(-E^+/RT)}{DD' - k_6(E)\,k_{-6}(E)}$$

$$k_{bi}(R8) = \kappa\frac{\sigma B_e Q_a^{\neq}}{hQ_{NH_2}Q_{OH}}\sum_{E0}^{\infty}\frac{k_8(E)\,k_6(E)\{G(E^+)\}\exp(-E^+/RT)}{DD' - k_6(E)\,k_{-6}(E)}$$

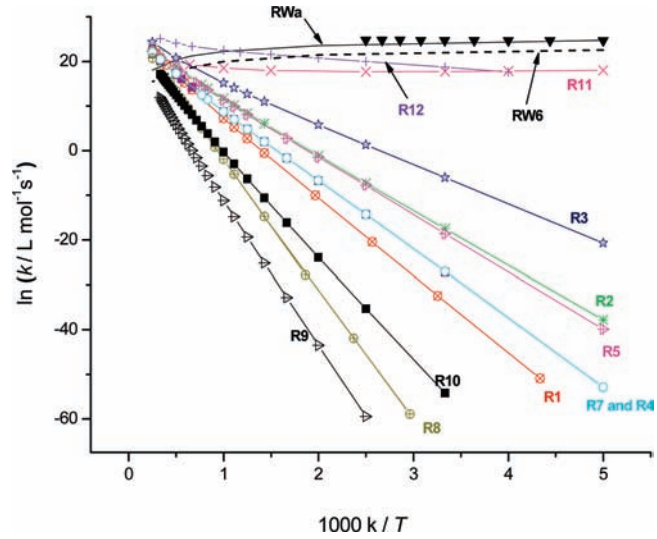

Figure 3. Arrhenius plot of the calculated rate constants for various channels at 760 Torr pressure of N_2. Solid line and dash lines represent the apparent rate of stabilization of NH_2OH and NH_3O adducts, (▼) from ref 4.

where k_{wa} and k_{w6} are the stabilization rate constants for NH_2OH^* and NH_3O^* under collision, respectively, $k_{bi}(R1)$−$k_{bi}(R8)$ are the rate constants for reactions R1−R8, respectively, and D and D′ are defined as:

$$D = k_{-a}(E) + w + k_1(E) + k_2(E) + k_3(E) + k_4(E) + k_5(E) + k_6(E)$$

$$D' = k_{-6}(E) + w + k_7(E) + k_8(E)$$

Here κ is the tunneling factor, B_e is the ratio of the electronic partition functions, h is the Planck constant, $Q_a^{\#}$ is the product of translational and rotational partition functions of the bottleneck for the entrance channel of NH_2OH^* intermediate, Q_{NH_2} and Q_{OH} are the partition functions of the reactants, $G(E^+_v)$ is the sum of vibrational states of the corresponding transition states at internal energy E_v^+, ω (= $Z\beta_c$[A]) is the collisional stabilization for energized intermediates NH_2OH^* and NH_3O^*, which β_c is the collision efficiency, and $k_x(E)$ is the microcanonical rate coefficient for the corresponding step in the energy range of E to $E + dE$, which is calculated from the quotient of the sum of states to the density of states in the corresponding step.

The tunneling correction factors κ were calculated according to a simple expression suggested by Shavitt.[41]

$$\kappa = 1 - \frac{1}{24}\left(\frac{h\nu^*}{k_B T}\right)^2\left(1 + \frac{k_B T}{E_0}\right)$$

where ν^* is the imaginary frequency of the activated complex at the top of the barrier, k_B and h are the Boltzmann and Planck constants, respectively, and E_0 is the barrier height corrected for zero-point energy for the hydrogen transfer steps.

Arrhenius plots for the rate constants of reactions R1−R8 and stabilization rate constants Rwa−Rw6 at high pressure limit are shown in Figure 3, which are compared with the available rate constants for the singlet surface in the literature, ref 4. Nonlinear least-squares fitting to the calculated rate constants at the CCSD(full) level in Figure 3 gave the following expression in L mol^{-1} s^{-1} unit.

$$k_{wa}^{\infty} = 4.0 \times 10^{19} \times T^{-3.23} \exp(-5.6 \text{ kJ mol}^{-1}/RT)$$

$$k_1 = 2.4 \times 10^{11} \exp(-151.9 \text{ kJ mol}^{-1}/RT)$$

$$k_2 = 5.7 \times 10^{10} \exp(-105.4 \text{ kJ mol}^{-1}/RT)$$

$$k_3 = 6.4 \times 10^{10} \exp(-77.1 \text{ kJ mol}^{-1}/RT)$$

$$k_4 = 6.410^{10} \exp(-131.1 \text{ kJmol}^{-1}/RT)$$

$$k_5 = 5.0 \times 10^{10} \exp(-107.9 \text{ kJ mol}^{-1}/RT)$$

$$k_{w6}^{\infty} = 5.56 \times 10^{19} \times T^{-3.59} \exp(-6.6 \text{ kJ mol}^{-1}/RT)$$

$$k_7 = 5.9 \times 10^{10} \exp(-129.9 \text{ kJ mol}^{-1}/RT)$$

$$k_8 = 1.9 \times 10^{12} \exp(-249.9 \text{ kJ mol}^{-1}/RT)$$

As shown in Figure 3, reactions R_{wa} and R_{w6} (stabilization of NH_2OH and NH_3O) are the major channels on the singlet surface in this system, as predicted by Fagerstrom. Formation of NH_3 and $O(^1D)$, the products of reactions R8 and R9, are the least important products in this system, as revealed by Figure 2.

CVT Results for Reactions R9−R12. ***Computational Details.*** Reactions R9 and R10 on the singlet surface and reactions R11 and R12 on the triplet surface proceed by passing over the corresponding saddle points. As shown in Figure 2, the contributions of reactions R9 and R10 on the singlet surface are negligible in this system, where we did not include their rate constants in our RRKM-TS calculations. Canonical variation transition state theory (CVT) was used to calculate their rate constants.[42,43] The CVT rate constant, k^{CVT}, can be calculated at temperature T, by minimizing the generalized TST rate constant, $k^{GT}(T,s)$, as a function of s:

$$k^{CVT}(T) = \min_s k^{GT}(TS) = \sigma \frac{k_B T}{h} \frac{Q^{GT}(T, s^{CVT})}{Q^R(T)} \times \exp\left[\frac{-V_{MEP}(s^{CVT})}{k_B T}\right]$$

where s is the arc length along the MEP measured from the saddle point; s^{CVT} is the value of s at which $k^{GT}(T,s)$ has a minimum, σ is the reaction path degeneracy; k_B and h are the Boltzmann and Planck constants, respectively, V_{MEP} (s^{CVT}) is the classical MEP potential at $s = s^{CVT}$, and $Q^{GT}(T, s^{CVT})$ and $Q^R(T)$ are the internal (rotational, vibrational, and electronic) partition functions of the generalized transition state at $s = s^{CVT}$ and reactants, respectively. The Page−McIver algorithm was used to follow the minimum energy path (MEP).[44] We performed a generalized normal-mode analysis projecting out frequencies at each point along the path.[45] With this information, we can calculate both the vibrational partition function along the MEP and the ground state vibrationally adiabatic potential curve

$$V_a^G(s) = V_{MEP}(s) + \varepsilon_{int}^G(s)$$

where $\varepsilon_{int}^G(s)$ is the zero-point energy at s from the generalized normal mode vibrations orthogonal to the reaction coordinate. A step size of 0.02 $(amu)^{1/2}$ bohr was used to calculate each individual point along the MEP, and a Hessian calculation was performed at each 0.06 $(amu)^{1/2}$ bohr. The adiabatic ground state potential $V_a^G(s)$, minimum energy path and zero-point energy for reactions R11 and R12 are shown in Figure 4.

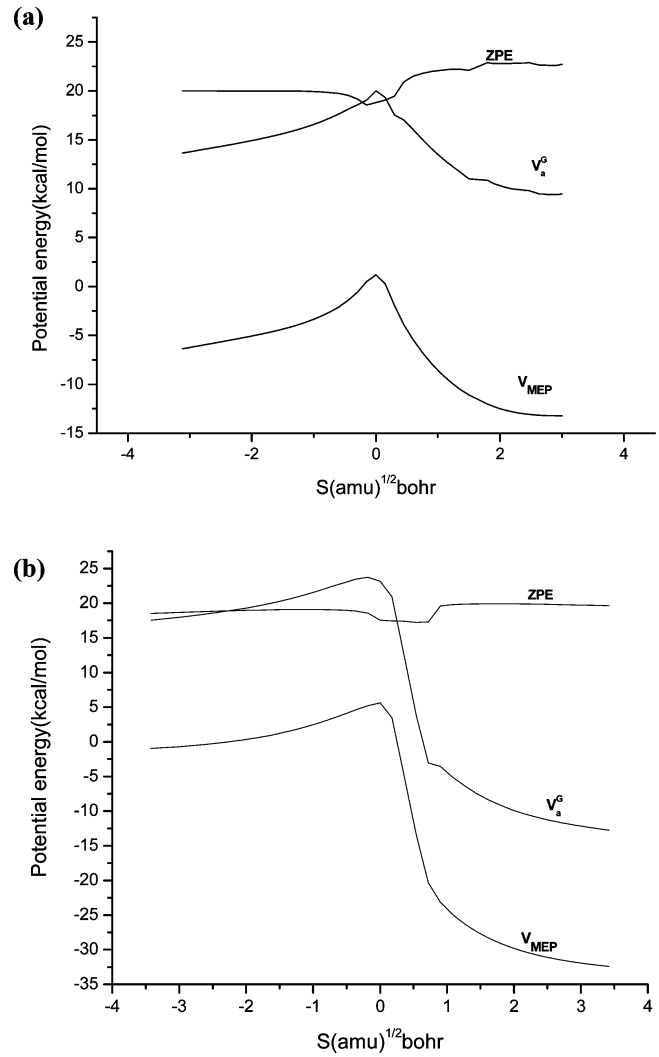

Figure 4. Variation of the vibrationally adiabatic ground-state potential $V_a^G(s)$, minimum energy path (MET), and zero-point energy for reactions R11 (a), and R12 (b) at the MPWB1K level.

To account for the quantum effects on the motion along the reaction coordinate, k^{CVT} (T) is multiplied by a ground-state transmission coefficient, $\kappa^{CVT/G}$ (T), which accounts for tunneling and nonclassical reflection effects. The quantized rate constant is given by[46,47]

$$k^{CVT/Y}(T) = \kappa^{CVT/G}(T) k^{CVT}$$

Zero and small curvature tunneling approximations are used to calculate the rate constants.[48−50] Our results indicated that for all four reactions the CVT/SCT rate constants are in much better agreement with the literature values.

In performing the dynamics calculations for reactions R9−R11 the geometries of all the stationary points were optimized at the MPWB1K level of theory along with the 6-31+G(d,p) basis set. The intrinsic reaction coordinate or MEP was constructed at the MPWB1K /6-31+G(d,p) for low level and at the CCSD(T)/Aug-cc-pVTZ methods for high level corrections. To the best of our knowledge, no kinetic data is available for reactions R9 and R10. The CVT rate constants for reactions

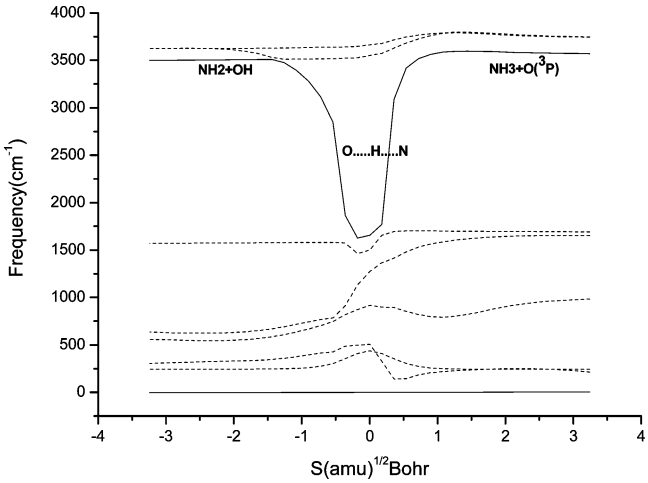

Figure 5. Variation of the frequencies along the MEP for reaction R11.

R9 and R10 are shown in Figure 3. For reaction R11 the MEP is starting from the saddle point geometry and going downhill toward the asymptotic reactant and product valleys to reach the van der Waals complexes $H_2N\cdots HO$ and $NH_3\cdots O$ in the reactants side and products side, respectively. Our CVT calculations revealed that for reaction R11 the calculated rate constants from MPWB1K data had better agreement with the reported results by Cohen et al.[7] and Baulch et al.[8] The van der Waals complexes $H_2N\cdots HO$ and $NH_3\cdots O$ are 17.6 and 18.4 kJ mol^{-1} (at the MPWB1K level) more stable than the reactants energy, respectively. To include the effect of multiple reflections above the van der Waals complexes on the rate of reaction, R11 a method of Hirschfelder and Wigner[51] as discussed by Miller[52] was used. To account for the effect of multiple reflections in the van der Waals complex well on the individual rate constants, the probability of the reaction flux passing through was calculated as follows:

$$P_{b\leftarrow a} = \frac{P_{b\leftarrow x}P_{x\leftarrow a}}{P_{b\leftarrow x} + P_{a\leftarrow x} - P_{b\leftarrow x}P_{a\leftarrow x}} = \frac{(N_2/N_x)(N_1/N_a)}{(N_2/N_x) + (N_1/N_x) - (N_2/N_x)(N_1/N_x)}$$

where $P_{x\leftarrow a}$, $P_{a\leftarrow x}$ and $P_{b\leftarrow x}$ are the probability of reactants forming a collision complex x, the probability that the complex decays back to the reactant(s), and the probability that the complex decays to the product(s), respectively, N_1, N_2, and N_x are the flux integrals through dividing surfaces S_1, S_2, and S_x, respectively.

The effect of multiple reflections above the van der Waals complex of $H_2N\cdots HO$ on the rate of channel R11 was found to be less than 1% at higher temperatures (>2000 K); however, this effect was found to be much stronger at low temperatures ($T < 600$ K). The multiple reflections above the van der Waals complex of $H_2N\cdots HO$ decreased the rate of reaction R11 by a factor of 0.62 at 200 K. This effect was found to be 0.84 at 1000 K. The same treatment on the effect of van der Waals complex $H_2NH\cdots O$ in the product side decreased the rate constant for the formation of $NH_3 + O(^3P)$, reaction R11, by a factor of 0.79 at room temperature. The variation of the normal mode vibrational frequencies along the MEP for reaction R11 is shown in Figure 5. As shown in Figure 5, all the frequencies, except one, do not change significantly during the reaction

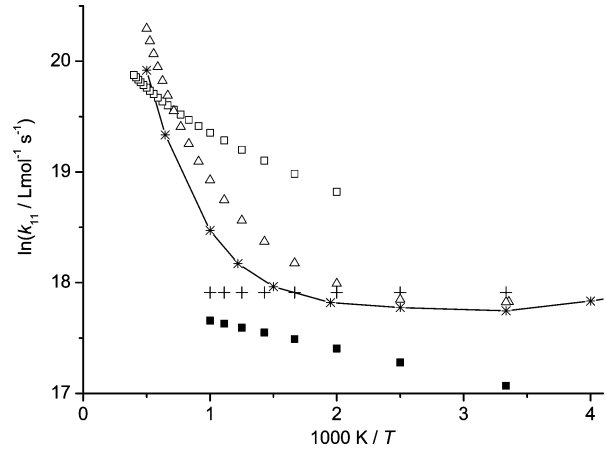

Figure 6. Arrhenius plot for reaction R11: (−*−) CVT results at the MPWB1K/6-311++(3df,3p) level; (Δ) from ref 7; (□) from ref 8; (■) from ref ; (+) from ref 17.

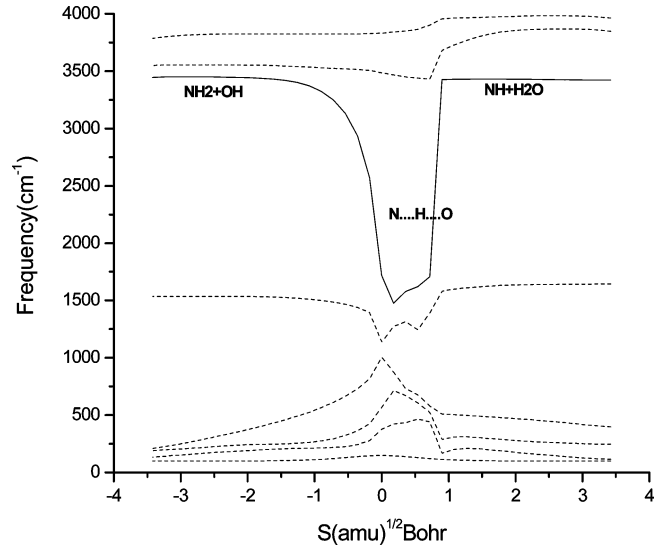

Figure 7. Variation of the frequencies along the MEP for reaction R12.

process from the reactants to the products. The frequency of $N\cdots H\cdots O$ stretching mode changes from 3610 cm^{-1} in the reactants side at $s = -3.12$ (amu)$^{1/2}$ bohr to 1621 cm^{-1} in the saddle point at $s = 0$, and then changes to 3520 cm^{-1} in the products side at $s = 3.2$ (amu)$^{1/2}$ bohr. The calculated rate constant for reaction R11 is compared with the available data in the literature in Figure 6 and is compared with the calculated rate constants of the other channels in this system in Figure 3. To the best of our knowledge no direct experimental data are available in the literature for the rate constant of reaction R11.

For reaction R12, the minimum energy path was calculated at the MP2/6-311++g(3df,3p) and the energies was corrected at the CCSD(full)/Aug-cc-pVTZ6 for high level calculations. Variation of the vibrationally adiabatic ground state potential $V_a^G(s)$, minimum energy path, and zero-point energy for reaction R12 at the MP2 level are shown in Figure 4. The variation of the normal mode vibrational frequencies along the MEP for reaction R12 is shown in Figure 7. As shown in Figure 7, the frequency of $N\cdots H\cdots O$ stretching mode changes from 3446 cm^{-1} in the reactants side at $s = -3.4$ (amu)$^{1/2}$ bohr to 1719 cm^{-1} in saddle point at $s = 0$ (amu)$^{1/2}$ bohr and reaches to 3422 cm^{-1} in the products side at $s = 3.4$ (amu)$^{1/2}$ bohr. The calculated rate constant for reaction R12 is compared with the available data in the literature in Figure 8 and is compared with

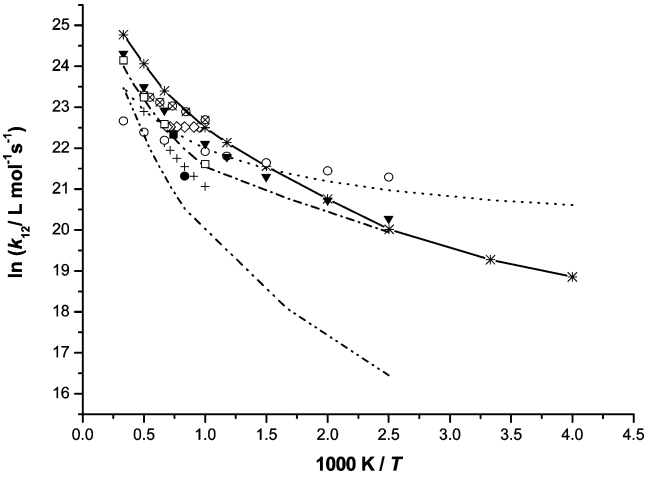

Figure 8. Arrhenius plot for reaction R12: (−*−) CVT results at the CCSD(full)/ Aug-cc-pVTZ level; (●) from ref 19; (○) from ref 18; (+) from ref 10; (■) from ref 20; (▼) from ref 15; (⊗) from ref 16; (◊) from ref 6; (•••) from ref 7; (□) from ref 21; (−••−••−••) from ref 11 at the UMP2/6-311G**; (−•−•−•−) line from ref 11 at the ump-sac4// UMP2/6-311G**.

the rate constants of the other channels in this system in Figure 3. As shown in Figure 8, our calculated rate constant for reaction R12 is in good agreement with the experimental data reported by Miller and Bowman.[15] No experimental data are reported for k_{12} at temperatures lower than 1000 K.

Nonlinear least-squares fitting to the calculated data in Figures 3 gave the following rate constant expressions for reactions R9−R12.

$$k_9 = 26.3 \times T^{2.36} \exp(-255.3 \text{ kJ mol}^{-1}/RT) \text{ L mol}^{-1}\text{s}^{-1}$$

$$k_{10} = 8.4 \times T^{2.79} \exp(-180.1 \text{ kJ mol}^{-1}/RT) \text{ L mol}^{-1}\text{s}^{-1}$$

$$k_{11} = 3.0 \times T^{2.41} \exp(+7.1 \text{ kJ mol}^{-1}/RT) \text{ L mol}^{-1}\text{s}^{-1}$$

$$k_{12} = 9.6 \times 10^3 \times T^{1.97} \times \exp(-2.8 \text{ kJ mol}^{-1}/RT)$$

The calculated rate constants of different channels are compared in Figure 3. Channel Rwa (stabilization of hydroxylamine), the most important channel in this system is in agreement with the conclusion made by Fagerstrom et al.,[4] although no product analysis was made in their study. According to our results, the next important channel is the stabilization rate constant for amine oxide NH_3O intermediate, Rw6, in agreement with the Mackie et al.[10] results. In our proposed mechanism, it is possible for NH_3O to dissociate into HNO + H_2 or rearrange to NH_2OH. As shown in Figure 3, the next two important channels in this system are reactions R11 and R12 that occur on the triplet surface. Both channels R8 and R9 for the formation of $NH_3 + O(^1D)$ are the minor channels in this system. Two channels exist for the formation of H_2O, reaction R2 and reaction R10. Most of the H_2O that is formed by channel R2 and channel R10 is negligible in this system.

Conclusion

The kinetics and mechanism of reaction $NH_2(^2B_1) + OH\ (^2\Pi)$ has been studied in detail by ab intio MO and direct dynamics calculations on both singlet and triplet surfaces. We presented the rate constant for 12 channels on the lowest singlet and triplet surfaces. Reactions R1−R8 proceed through chemically activated intermediates NH_2OH^* and NH_3O^* on the singlet surface. Microcanonical variational RRKM method was used to locate the position of the bottlenecks for those channels with no saddle point. A method base on the RRKM and TST was used to calculate the rate constants for reactions R1−R8. Canonical variational transition state theory along with the small-curvature tunneling approximation (CVT/SCT) was used to calculate the rate constants of direct H abstraction channels that proceed on the singlet or triplet surfaces.

To calculate the rate constants for those channels that proceed by passing through the energized adducts NH_2OH^* and NH_3O^*, strong collision assumption was used. Our results at lower temperatures predict the main channels on the singlet surface are the formation and stabilization of hydroxyl amine and amine oxide. No potential barrier exists for the formation of these energized intermediates. Energized intermediate NH_3O^* could be isomerized to NH_2OH easily; that could be the reason for not being detected experimentally until now. To the best of our knowledge, no direct observation of NH_3O has been reported to date, although its formation has been predicted theoretically.[10,32,33] At temperatures above 850 K the most important channel is the formation of H_2O on the triplet surface, reaction R12. Formation of NH_3 and H_2O on the triplet surface (reactions R11 and R12) are the next important paths in this system because of having low barriers relative to the barriers of the other channels, as shown in Figure 2.

The effect of multiple reflections over the van der Waals complexes in both reactants side and products side was calculated and found to decrease the rate constant of reaction R11 by a factor of 0.49 at room temperature. The reported rate constant for reaction R11 is corrected for this effect.

As mentioned by Wang et al.,[13] formation of $H_2NH\cdots O$ van der Waals complex on the singlet surface along channel R9 is a local minimum just at the CAS level of theory. We were not able to locate such a complex at the other levels of theory.

Energized intermediate NH_3O^* could be isomerizes to NH_2OH easily that could be the reason for not being detected experimentally until now. Formation of NH_3 and H_2O on the triplet surface (reactions R11 and R12) are the next important paths in this system because of having low barriers relative to the barriers of the other channels, as indicated in Figure 2.

Acknowledgment. The financial support of the Research Council of Shiraz University is acknowledged.

References and Notes

(1) McConell, J. C. *J. Geophys. Res.* **1973**, *78*, 7812. Report of the NASA working group on troposphere program planning: *NASA Reference Publication*; NASA: Washington, DC, 1980; p 1062.

(2) Johnson, R. D., III. *Computational Chemistry Comparison and Benchmark DataBase*, http://srdata.nist.gov/cccbdb/exp2.asp.

(3) Lyon, R. K. Environ. *Sci. Technol.* **1987**, *21*, 231.

(4) Fagerstrom, K.; Jodkowski, J. T.; Lund, A.; Ratajczak, E. *Chem. Phys. Lett.* **1995**, *236*, 103.

(5) Gericke, K. H.; Loch, M.; Schmidt, F.; Comes, F. J. *J. Chem. Phys.* **1994**, *101*, 1988.

(6) Kimball-Linne, M. A.; Hanson, R. K. *Combust. Flame* **1986**, *64*, 337.

(7) Cohen, N.; Westberg, K. R. *J. Phys. Chem. Ref. Data* **1991**, *20*, 1211.

(8) Baulch, D. L.; Cobos, C. J.; Cox, R. A.; Esser, C.; Frank, P.; Just, T.; Kerr, J. A.; Pilling, M. J.; Troe, J.; Walker, R. W.; Warnatz, J. *J. Phys. Chem. Ref. Data* **1992**, *21*, 411.

(9) Dean, A. M.; Bozzelli, J. W. In *Gas-Phase Combustion Chemistry*; Gardiner, W. C., Jr., Ed.; Springer-Verlag: New York, 2000; p 125.

(10) Mackie, J. C.; Bacskay, G. B. *J. Phys. Chem. A* **2005**, *109*, 11967.

(11) Xu, Z.-F.; Fang, D.-C.; Fu, X.-Y. *Theor. Chem. Acc.* **2000**, *104*, 7.

(12) Shu, J.; Lin, J. J.; Wang, C. C.; Lee, Y. T.; Yang, X. *J. Chem. Phys.* **2001**, *115*, 842.

(13) Wang, L.; Mebel, A. M.; Yang, X.; Wang, X. *J. Phys. Chem. A* **2004**, *108*, 11644.
(14) Hart, B. T. *Aus. J. Chem.* **1976**, *29*, 231.
(15) Miller, J. A.; Bowman, C. T. *Prog. Energy Combust. Sci.* **1989**, *15*, 287.
(16) Salimian, S. S.; Hanson, R. K.; Kruger, C. H. *Combust. Flame* **1984**, *56*, 83.
(17) Hampson, R. F. Report No. FAA-EE-80-17; U.S. Dept. of Transport, 1980.
(18) Dean, A. M.; Hardy, J. E.; Lyon, R. K. *19th Int. Symp. Combust.* **1982**, 97.
(19) Branch, M. C.; Kee, R. J.; Miller, J. A. *Combust. Sci. Technol.* **1982**, *29*, 147.
(20) Niemitz, K. J.; Wagner, H. G.; Zellner, R. *Z. Phys. Chem.* **1981**, *124*, 155.
(21) Zebetta, E. C.; Kilpinen, P.; Hupta, M.; Stahl, K.; Leppalahti, J.; Cannon, M.; Nieminen, J. *Energy Fuels* **2000**, *14*, 751.
(22) Baulch, D. L.; Drysdale, D. D. ; Horne, D. G.; Lloyd, A. C. *Evaluated Kinetic Data for High Temperature Reactions;* Butterworths: London, 1973; Vol. 2, p 483.
(23) Diau, E. W.-G.; Tso, T.-L.; Lee, Y.-P. *J. Phys. Chem.* **1990**, *94*, 5261.
(24) Fenimore, C. P. *Combust. Flame* **1980**, *37*, 245.
(25) Dean, A. M. *J. Phys. Chem.* **1985**, *89*, 4600.
(26) Mousavipour, S. H.; Saheb, V. *Bull. Chem. Soc. Jpn.* **2007**, *80*, 1901.
(27) Frisch, M. J. ; Trucks, G. W.; Schlegel, H. B.; Scuseria, G. E.; Robb, M. A. J.; Cheeseman, R. V.; Zakrzewski, G. J.; Montgomery, A., Jr.; Stratmann, R. E.; Burant, J. C.; Dapprich, S.; Millam, J. M.; Daniels, A. D.; Kudin, K. N.; Strain, M. C.; Farkas, O.; Tomasi, J.; Barone, V.; Cossi, M.; Cammi, R.; Mennucci, B.; Pomelli, C.; Adamo, C.; Clifford, S.; Ochterski, J.; Petersson, G. A.; Ayala, P. Y.; Cui, Q.; Morokuma, K.; Malick, D. K.; Rabuck, A. D.; Raghavachari, K.; Foresman, J. B.; Cioslowski, J.; Ortiz, J. V.; Stefanov, B. B.; Liu, G.; Liashenko, A.; Piskorz, P.; Komaromi, I.; Gomperts, R.; Martin, R. L.; Fox, D. J.; Keith, T.; Al-Laham, M. A.; Peng, C. Y.; Nanayakkara, A.; Gonzalez, C.; Challacombe, M.; Gill, P. M. W.; Johnson, B.; Chen, W.; Wong, M. W.; Andres, J. L.; Head-Gordon, M.; Replogle E. S.; Pople, J. A. *Gaussian 03,* revision B.01, Gaussian, Inc.: Pittsburgh, PA, 2003.
(28) Becke, A. D. *J. Chem. Phys.* **1993**, *98*, 5648. Becke, A. D. *J. Chem. Phys.* **1992**, *96*, 2155. Becke, A. D. *J. Chem. Phys.* **1992**, *97*, 9173.
(29) Lee, W.; Yang, W.; Parr, R. G. *Phys. Rev. B* **1988**, *37*, 785.
(30) Yamamoto, N.; Vreven, T.; Robb, M. A.; Frisch, M. J.; Schlegel, J. B. *Chem. Phys. Lett.* **1996**, *250*, 373, and references therein.
(31) Gonzalez, C.; Schlegel, H. B. *J. Phys. Chem.* **1990**, *94*, 5523.
(32) Baulch, D. L.; Campbell, I. M.; Hainsworth, R. *J. Chem. Soc., Faraday Trans. 1* **1984**, *80*, 2525.
(33) Kirby, A. J.; Davies, J. E.; Brandão, T. A. S.; da Silva, P. F.; Rocha, W. R.; Nome, F. *J. Am. Chem. Soc.* **2006**, *128*, 12374.
(34) Baer, T.; Hase, W. L. *Unimolecular Reaction Dynamics: Theory and Experiments*; Oxford University Press: New York, 1996.
(35) Corchado, J. C.; Chuang, Y.-Y.; Coitino, E. L.; Truhlar, D. G. *GAUSSRATE,* version 9.1/P9.1-G03/G98/G94; Department of Chemistry and Supercomputer Institute, University of Minnesota: Minneapolis, MN, 2003.
(36) Corchado, J. C.; Chuang, Y.-Y.; Fast, P. L.; Villa, J.; Hu, W.-P.; Liu, Y.-P.; Lynch, G. C.; Nguyen, K. A. F. Jackels, C. F.; Melissas, V. S.; Lynch, B. J.; Rossi, I.; Coitino, E. L.; Fernandez Ramos, A.; Pu, J.; Albu, T. V.; Steckler, R.; Garrett, B. C.; Isaacson, A. D.; Truhlar, D. G. *POLYRATE,* version 9.3; Department of Chemistry and Supercomputer Institute, University of Minnesota: Minneapolis, MN, 2003.
(37) Zhu, L.; Chen, W.; Hase, W. L. *J. Phys. Chem.* **1993**, *97*, 311.
(38) Zhu, L.; Hase, W. L. *QCPE Program 644; Quantum Chemistry Program Exchange*; Indiana University: Bloomington, IN, 1993.
(39) Börjesson, L. E. B.; Nordholm, S. *J. Phys. Chem.* **1995**, *99*, 938.
(40) Tardy, D. C.; Rabinovitch, B. S.; Whitten, G. Z. *J. Chem. Phys.* **1968**, *48*, 1427.
(41) Shavitt, I. *J. Chem. Phys.* **1959**, *31*, 1359.
(42) Truhlar, D. G.; Isaacson, A. D.; Garrett, B. C. In *Theory of Chemical Reaction Dynamics*; Baer, M., Ed.; CRC Press: Boca Raton, 1985; Vol. 4, p 65.
(43) Truhlar, D. G.; Garrett, B. C. *Annu. Rev. Phys. Chem.* **1984**, *35*, 159.
(44) Page, M.; McIver, J. W. *J. Chem. Phys.* **1988**, *88*, 922.
(45) Miller, W. H.; Handy, N. C.; Adams, J. E. *J. Chem. Phys.* **1980**, *72*, 99.
(46) Truhlar, D. G.; Isaacson, A. D.; Garrett, B. C. In *The Theory of Chemical Reaction Dynamics*; Baer, M., Ed.; CRC Press: Boca Raton, FL, 1985; Vol. 4, pp 65−137.
(47) Garrett, B. C.; Truhlar, D. G.; Grev, R. S.; Magnuson, A. W. *J. Phys. Chem.* **1980**, *84*, 1730.
(48) Truhlar, D. G.; Kuppermann, A. *J. Am. Chem. Soc.* **1971**, *93*, 1840.
(49) Liu, Y.-P.; Lynch, G. C.; Truong, T. N.; Lu, D.-h.; Truhlar, D. G.; Garrett, B. C. *J. Am. Chem. Soc.* **1993**, *115*, 2408.
(50) Liu, D.-h.; Truong, T. N.; Melissas, V. S.; Lynch, G. C.; Liu, Y.-P.; Garrett, B. C.; Steckler, R.; Isaacson, A. D.; Rai, S. N.; Hancock, G. C.; Lauderdale, J. C.; Joseph, T.; Truhlar, D. G. *Comput. Phys. Commun.* **1992**, *71*, 235.
(51) Hirschfelder, J. O.; Wigner, E. *J. Chem. Phys.* **1939**, *7*, 616.
(52) Miller, W. H. *J. Chem. Phys.* **1976**, *65*, 2216.

JP905197H